Journal of Electroceramics 3:4, 377–385, 1999

Dielectric Properties of La^{3+} Doped $Sr_{0.3-3y/2}La_y\ Ba_{0.7}Nb_2O_6$ Ceramics Prepared under Different Sintering Conditions*

FIDEL GUERRERO,[1] HARVEY AMORÍN,[2] JORGE J. PORTELLES,[2,3] ABEL FUNDORA,[2,3] JESÚS M. SIQUEIROS,[3] GUSTAVO A. HIRATA[3] & SARA AGUILERA[4]

[1]*Facultad de Ciencias Naturales, Universidad de Oriente, Santiago de Cuba 90500, Cuba.*
[2]*Facultad de Física-IMRE, Universidad de la Habana, Vedado, La Habana 10400, Cuba.*
[3]*Centro de Ciencias de la Materia Condensada, Universidad Nacional Autónoma de México, Apartado Postal 2681, Ensenada, Baja California, México, 22800.*
[4]*Facultad de Ciencias, Universidad Católica del Norte, Avenida Angamos 0610, Casilla 1280, Antofagasta, Chile.*

Submitted December 28, 1998; Revised May 4, 1999; Accepted May 7, 1999

Abstract. A study of the dielectric properties of the Lanthanum doped $Sr_{0.3}Ba_{0.7}Nb_2O_6$ (SBN30) ceramic according to the stoichiometric formulation $Sr_{0.3-3y/2}La_yBa_{0.7}Nb_2O_6$ with $y = 0.01$, 0.03 and 0.05, and the influence of the sintering conditions is reported. The XRD shows single phase compounds for $Sr_{0.285}La_{0.01}Ba_{0.7}Nb_2O_6$ (LSBN1) and $Sr_{0.255}La_{0.03}Ba_{0.7}Nb_2O_6$ (LSBN3) ceramics, both samples having similar microstructure, densification and dielectric properties. The density increases linearly with *ln t*, where *t* is the sintering time, and the values of the maximum ferroelectric peaks of the permittivity increase steadily with *t*. Using the Bruggeman model to estimate the theoretical permittivity, it is concluded that the magnitude of the experimental permittivity peaks are mainly affected by the volume fraction of porosity of the samples. In this study we also establish that pore diffusion mechanisms behave according to the Ginstling-Brownshtein equation. For the $Sr_{0.225}La_{0.05}Ba_{0.7}Nb_2O_6$ (LSBN5) sample, XRD analysis reveals the presence of isostructural compounds of the intermediate phases $BaNb_2O_6$ and $SrNb_2O_6$, and the dielectric properties start to deteriorate. This fact indicates the existence of a solubility limit of Lanthanum ions in the SBN solid solution.

Keywords: ferroelectric ceramics, dielectric properties, microstructure, densification

1. Introduction

The $Sr_xBa_{1-x}Nb_2O_6$ (SBN) system was reported as a ferroelectric material by Francombe in 1960 and ever since applications have been widely studied in the literature [1]. The system exhibits very good ferroelectric [2] and electrooptic properties, as well as a strong photorefractive effect [3]. Moreover, SBN possesses excellent pyroelectric properties with very fast response times [4].

*This work was partially sponsored by CoNaCyT Proj. No. 26314 E and 3025P-E9607 and DGAPA Proj. No. IN115098. A. Fundora thanks the Foreign Ministry of México for their support.

The ferroelectric properties of the SBN family have been studied mainly in single crystal form, grown mostly by the Czochralsky technique[1] and their dependence on the Sr/Ba concentration ratio has been established [2]. Liu et al. [5] showed that when SBN 0.5/0.5 is doped with rare earth cations, the physical properties are modified according to the cationic substitution. A reduction of the Curie temperature and the enhancement of the pyroelectric coefficient to twice the value of the undoped SBN has been reported.

In spite of their good properties, the growth of the SBN crystals requires costly installations. The phase diagram of this system is complicated [3] and, in some instances the compositions turn out to be

inhomogeneus, often resulting in drastic variations of the electrical and optical properties.

Polycrystalline $BaTiO_3$, [6,7] PZT, [8–10] PMN-PT [11,12] and other compounds have been widely used in the ceramic form [3] since they show, in many cases, properties similar to those of the corresponding single crystals. Similar results have been found by us in SBN ceramics [13,14]. Moreover, ceramics may be prepared in a large composition range and it is possible to adjust the characteristics of the material for different applications [15] in addition to its relatively simple manufacture process.

For some compositions, it has been found convenient (when the Ba content is greater than 0.66) to obtain this compound in ceramic form [16–18]. The addition of small amounts of rare-earth dopants and other ions has been the usual way to change the microstructure of the compounds, in some cases with an increase of the diffusion and densification rates [19] and in others with an increase of the grain size [20].

The SBN 0.3/0.7 composition presents the largest pyroelectric coefficient of the SBN system. However, its Curie temperature is over 200°C. The Lanthanum doping of the SBN ceramics has helped to decrease the SBN transition temperature, thereby improving the dielectric and pyroelectric properties of the material at room temperature [5,13].

With the purpose of obtaining new ceramic materials with good pyroelectric properties, this work is dedicated to the study of the effects of the sintering process and the influence of the Lanthanum content in the $(Sr_{0.3-3y/2}La_yBa_{0.7})Nb_2O_6$ ceramic system.

2. Experimental Procedure

The composition of the studied system is given by $(Sr_{0.3-3y/2}La_yV_{y/2})Ba_{0.7}Nb_2O_6$ where V stands for induced vacancies. The samples were prepared by a conventional ceramic technique by mixing the proper amounts of high purity reactants, $BaCO_3$, $SrCO_3$, La_2O_3 and Nb_2O_5, in a agate mortar with ethyl alcohol for 2 h. To examine the influence of the Lanthanum content on the properties of the sintered material for $y = 0.01$, 0.03 and 0.05 labeled LSBN1, LSBN3 and LSBN5 respectively, the powders were calcined for 2 h at 900°C, and then uniaxially die-pressed at 612 Mpa, into 10 mm in diameter disks. Finally, the samples were sintered at 1400°C from 1 to 5 h.

After the sintering process, the density of the samples was obtained by measuring their volume and weighing them. The temperature dependence of the dielectric constant was experimentally determined with a personal computer controlled RLC bridge (PHILIPS PM 6303) at a frequency of 1 kHz, using diffused silver electrodes.

The sintered samples were examined by XRD in a Philips-PW-1821 diffractometer. The crystalline phases were identified using CuKα radiation and a 0.05°/step. Peak indexation was realized with the PC-APD software [21]. For the determination of the lattice parameters, scans in the 2θ range of 10° to 150° with a 0.01 step were performed. The integral intensity of each reflection was analyzed by X-Ray Powder Diffraction Analysis (XPAS). The microstructure was obtained using a Jeol JSM-5300 scanning electron microscope.

3. Results and Discussion

3.1. XRD Analysis

The X-ray diffraction spectra of the LSBN1 ceramic, for sintering times from 1 to 5 h, is shown in Fig. 1. The Miller indices of the main reflections are represented in this figure showing a single phase material, isostructural with the SBN phase. The incorporation of Lanthanum into the lattice must lead to a deformation of the SBN structure, according to previously reported results [22]. A question of interest that remains, could be the rate at which this incorporation occurs.

From Fig. 1 we see that there is basically no shift of the reflection angles with the sintering time. This fact suggests that the incorporation of Lanthanum in certain crystallographic sites of the SBN structure and the corresponding lattice deformation, occur early in the sintering process. The integral intensity of some of the reflections increases in different way with the increase of the sintering time, suggesting a possible selective location of the ions at certain crystallographic sites of the structure. Similar results were also found for the LSBN3 and LSBN5 samples in terms of the sintering time dependence of the phase reflection angles.

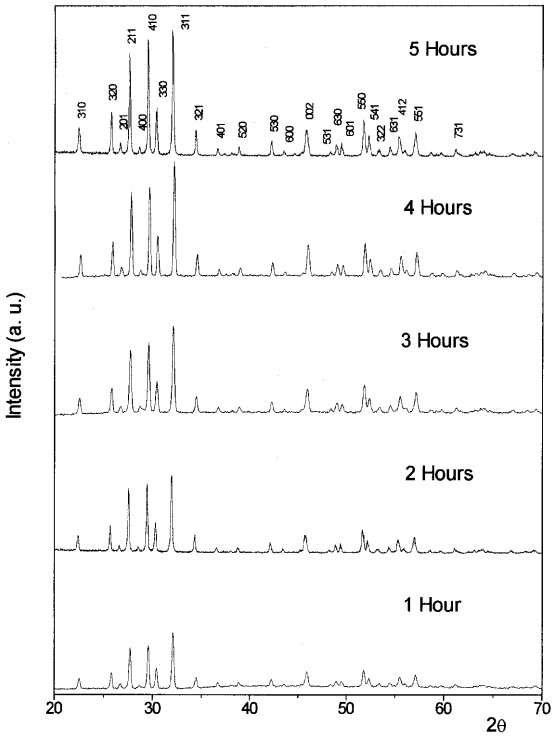

Fig. 1. XRD of the $Sr_{0.285}La_{0.01}Ba_{0.7}Nb_2O_6$ (LSBN1) ceramic with sintering times in the range of 1 to 5 h, showing, in all cases, a single phase compound.

Figure 2 shows the XRD patterns of the three samples (LSBN1, LSBN3 and LSBN5) sintered for 5 h. As is well known, the formation of the SBN compound from the raw materials ($SrCO_3$, $BaCO_3$ and Nb_2O_5) is obtained through the intermediate phases $BaNb_2O_6$ and $SrNb_2O_6$ [18]. For comparison purposes, we also include the XRD patterns of SBN calcined at 900°C for 2 h, where intermediate phases are observed. One should notice that LSBN1 and LSBN3 patterns are quite similar. For LSBN5 however, besides the SBN phase reflections, the corresponding XRD pattern shows some small reflections associated to additional phases present in the ceramic which proved to be isostructural with the intermediate phases of the SBN compound. This result indicates that LSBN5 is not of single phase type as the LSBN1 and LSBN3 ceramics. Since the crystal structure was found to be independent of the sintering time, for the times used in this experiment, the presence of additional phases must be due to the existence of a solubility limit of the La ions into the SBN structure.

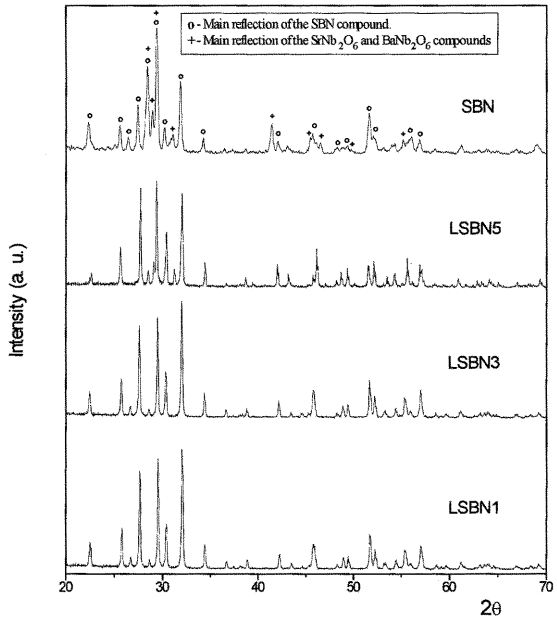

Fig. 2. XRD of the $(Sr_{0.3-3y/2}La_yBa_{0.7})Nb_2O_6$ ceramic sintered for 5 h and of calcined SBN at 900 °C where intermediate $SrNb_2O_6$ and $BaNb_2O_6$ phases are observed. We can see in the $Sr_{0.285}La_{0.01}Ba_{0.7}Nb_2O_6$ (LSBN5) XRD pattern smaller peaks associated to the additional phases.

The above mentioned PC-APD software was used to estimated the lattice parameters shown in Table 1 for different Lanthanum content samples sintered for 5 h. There is an increase of the **a** parameter with the Lanthanum content while **c** remains constant within the considered measurement error [21]. This behavior agrees well with that reported by Maciolek et al. for the La doped SBN50 system [22]. Estimated data for LSBN1 sintered for 1 and 5 h (see also Table 1) indicate that there is no variation of the lattice parameters indicating no deformation of the structure with the sintering time. Room temperature dielectric losses $(\mathrm{Tan}\,\delta_o)$ at 1 kHz are also included in Table 1 for the samples sintered for 5 h showing the smallest value for the LSBN3 composition.

3.2. Microstructure

The microstructure of the LSBN1 sintered for 1, 3 and 5 h is shown in Fig. 3. The grain size has a homogeneous distribution, and intergranular voids (pores) are observed. The pore concentration decreases with sintering time. For 3 and 5 h of sintering, the remaining pores are enclosed between

Table 1. Lattice parameters, lattice volumes, theoretical density and and room temperature dielectric losses ($\mathrm{Tan}\,\delta_o$) at 1 kHz, of the $Sr_{0.3-3y/2}La_yBa_{0.7}Nb_2O_6$ system

Sample	Sintering time (h)	a (Å) $\pm$ 0.005	c (Å) $\pm$ 0.005	V_c(Å^3)	Theoretical density (g/cm^3)	Tan δ_o
LSBN1	1 h	12.51	3.97	621	5.43	—
LSBN1	5 h	12.50	3.97	621	5.43	0.074
LSBN3	5 h	12.52	3.97	622	5.40	0.034
LSBN5	5 h	12.54	3.97	624	5.38	0.134

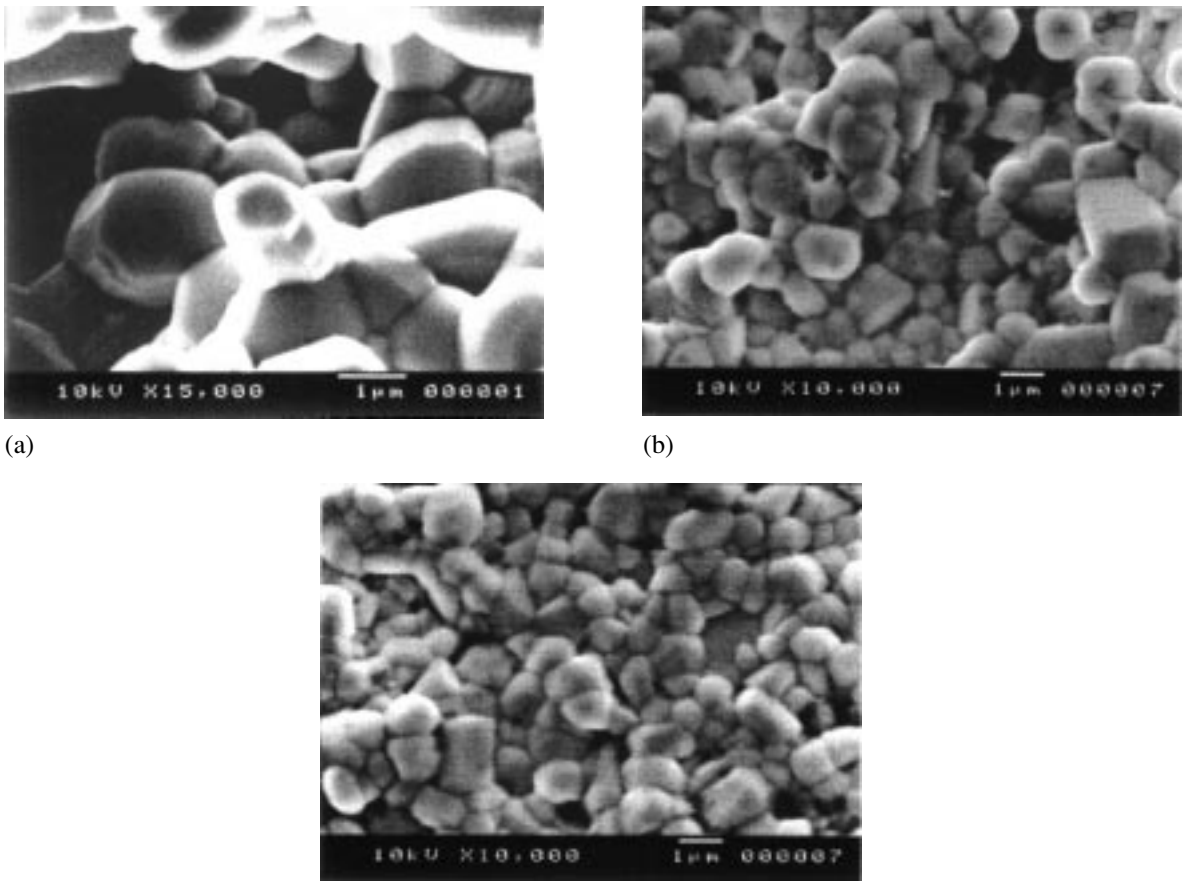

Fig. 3. Microstructure of the $Sr_{0.285}La_{0.01}Ba_{0.7}Nb_2O_6$ (LSBN1) ceramic, sintered for (a) 1, (b) 3 and (c) 5 h, showing, for 3 and 5 h of sintering, that remaining pores are enclosed between three or four grains, indicating to be the final step of the sintering process.

three or four grains, indicative of the final step of the sintering process [23] corresponding to a large decrease in the densification rate (see Fig. 4).

Similar microstructure features were obtained for the LSBN3 and LSBN5 ceramics. In these two cases, however, the final step of the sintering process was found to start after 5 h of firing time. The estimated grain size remained in the range of 1–2 μm and there was no evidence of grain size variations either with sintering time, in agreement with the observations of Nishiwaki et al. [16] in the SBN ceramic with Sr/Ba = 0.3/0.7 ratio, or with Lanthanum content. In particular, for LSBN5 where, according to the XRD results a multimodal grain size distribution should be expected, only a single grain size distribution could be resolved from the SEM micrographs.

3.3. Density and Porosity

The dependence of the density ρ with sintering time of the LSBN ceramic system is shown in Fig. 4 for different La content. For the LSBN1 ceramic, ρ increases from 3.82 g/cm^3 (70% of theoretical density ρ_{th}) to 5.32 g/cm^3 (98% ρ_{th}), following a logarithm function of the sintering time, as predicted by Coble's model [23].

The densification rates calculated over different time intervals from the slope of the curve, decreased from 0.66 with correlation coefficient $r = 0.994$ for 1 to 3 h, to 0.15 with $r = 0.993$ for 3 to 5 h. This fact clearly indicates that the densification rate of the material is reduced with increasing sintering time. A simple but reasonable assumption that the relation $d\rho/dt$ is proportional to the diffusion coefficient D, as proposed by Coble [23], allows us to assume here that the diffusion process decreases also with increasing sintering time. This reduction is explained by the fact that in the final step of the sintering process, as we pointed out above from our microstructure observation, pores are enclosed between grains and cannot therefore move freely.

From Fig. 4 it is also observed that the densities decrease as the La content increases, and is especially low for LSBN5. This result is more clearly shown in Fig. 5 for different sintering times where a contrasting behavior with previous observations on PLZT [24] is

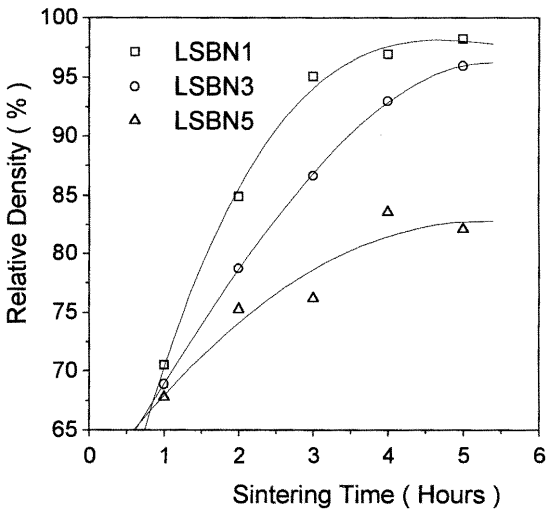

Fig. 4. Dependence of the relative density with sintering time for the $Sr_{0.3-3y/2}La_yBa_{0.7}Nb_2O_6$ ceramic system following, in all cases, a logarithm function of sintering time, as predicted by Coble's model[23].

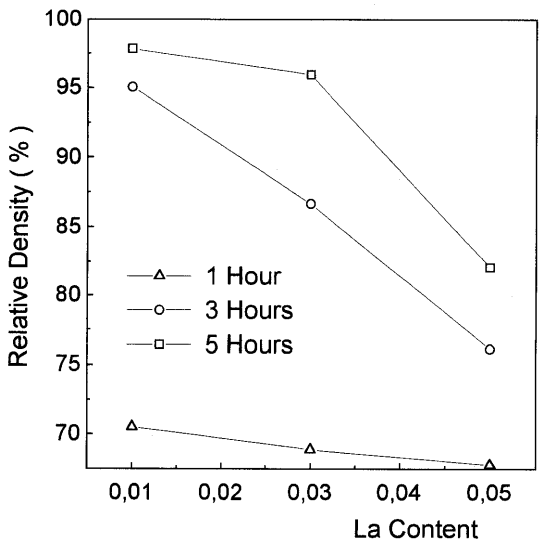

Fig. 5. Dependence of the relative density with La content for the $Sr_{0.3-3y/2}La_yBa_{0.7}Nb_2O_6$ ceramic system on sintering times.

seen, where the density grows as the La content increases. One reason for such behavior may be the fact that, in our case, the vacancies introduced by the doping (La) are bound to the doping ions and cannot move freely through the crystal to expedite mass transfer. The number of these bound vacancies increases with the rise of La content with a $y/2$ ratio according to the chemical composition $(Sr_{0.3-3y/2}La_yV_{y/2})Ba_{0.7}Nb_2O_6$. Moreover, for LSBN5, one must take into account that the presence of additional phases with lower densities than the SBN may lead to a decrease of the resulting material density.

For a sintering time of 3 h, a dense material with porosity values below 5% was obtained for the LSBN1 ceramic, while LSBN3 required 5 h to reach such degree of densification.

3.4. Diffusion Mechanism of the Pores

The general properties of the $Sr_{0.3-3y/2}La_yBa_{0.7}Nb_2O_6$ ceramic system as a function of their thermal history are summarized in Table 2. For each ceramic composition, the maximum values of the permittivity increase monotonically with sintering time. In the majority of cases, such an increase of permittivity can have three major causes: (1) an increase of the number of dipoles caused by a higher doping [24], (2) grain size increase [25] and (3) the decrease of the porosity

Table 2. General characteristics of the sintering process of the LSBN ceramic system

Sintering conditions	Density (g/cm^3)	Porosity (%)	Measured permittivity maxima	Permittivity maxima without pores	Transition temperature (°C)
		LSBN1			
1400°C—1 h	3.82	29.4	1198	1932	172
2 h	4.60	15.1	1517	1920	172
3 h	5.15	4.9	1752	1917	171
4 h	5.25	3.1	1818	1911	171
5 h	5.32	1.8	1852	1910	170
		LSBN3			
1 h	3.72	31.1	1186	1990	135
2 h	4.25	21.3	1413	1987	135
3 h	4.68	13.3	1597	1965	132
4 h	5.02	7.0	1773	1974	130
5 h	5.18	4.1	1851	1970	128
		LSBN5			
1 h	3.65	32.2	411	—	76
2 h	4.05	24.8	430	—	79
3 h	4.10	23.9	499	—	76
4 h	4.50	16.4	519	—	76
5 h	4.42	17.9	567	—	74

[25]. The first cause was discarded because no shifts in the Curie temperature are observed for any composition, reiterating the fact that all the doping is incorporated into the SBN lattice within the first hour of sintering time.

The existence of different models relating the dielectric constant with the volumetric fraction of pores is well documented [26]. Among them, the Bruggeman model is the one that better fits our experimental results:

$$\varepsilon^* = \varepsilon(1 - 3p/2) \qquad \text{(connectivity 3—3)} \qquad (1)$$

$$\varepsilon^* = \varepsilon(1 - p)/(1 + p/2) \qquad \text{(connectivity 3—0)} \qquad (2)$$

where ε and ε^* are the zero porosity permittivity and the measured permittivity, respectively, and p is the volume fraction of the porosity. The model considers the existence of two phases, one corresponding to the material and the other to the pores and assume that the spherical shaped pores are embedded in the LSBN phase. From expressions (1) and (2) it is possible to extract the poreless dielectric constant $\varepsilon(p = 0)$. Additionally, from microstructure analysis of the samples, we saw that pores are interconnected in the samples with 1 and 2 h of sintering time but for the samples with 3 to 5 h, the pores are enclosed between three or four grains and not interconnected. This result allows us to use for our experiment the 3–3 connectivity expression for 1 and 2 h of sintering time and the 3–0 connectivity expression for the 3–5 h samples.

Figure 6 shows the difference between ε^* and $\varepsilon(p = 0)$ calculated from the Bruggeman model for the LSBN1 ceramic for different sintering times. In all the cases it is observed that the theoretical dielectric constant is larger than ε^*, this difference becoming larger above the transition temperature.

The dependence of the maximum dielectric constant without pores and of the measured dielectric constant with porosity is shown in Fig. 7. It can be seen that ε stays approximately constant. This result clearly suggests that the increase in ε^* during the sintering of the material is due to a reduction in the porosity rather than to a grain size variation, in agreement with our microstructure observations.

During the sintering process mass transport and the principal mechanisms that take place are of diffusive character [26]. With the objective of determining the possible mechanism governing the diffusive dynamics of the pores during the sintering of the LSBN1 ceramics, the dependence of the maximum value of the dielectric constant with the porosity was examined. A normalization parameter $\alpha(0 < \alpha < 1)$ is defined as

$$\alpha_i = [\varepsilon(t_i) - \varepsilon(t_o)]/[\varepsilon(t_f) - \varepsilon(t_o)] \qquad (3)$$

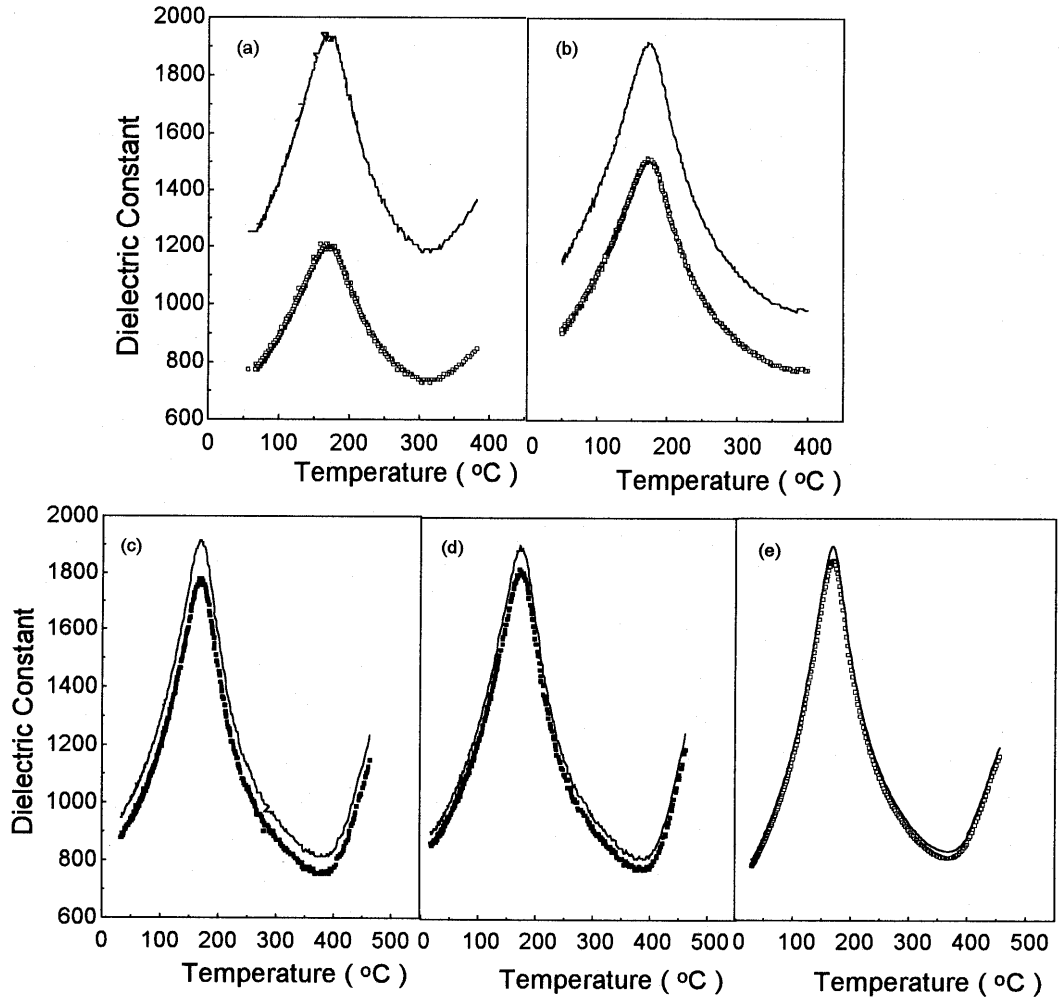

Fig. 6. Measured ε^* and calculated $\varepsilon(p = 0)$ permittivity using Bruggeman's model for the $Sr_{0.285}La_{0.01}Ba_{0.7}Nb_2O_6$ (LSBN1) ceramic sintered during (a) 1, (b) 2, (c) 3, (d) 4 and (e) 5 h.

where t_i, t_o and t_f are interest, initial and final times respectively. The resulting α_i values as functions of the sintering time showed a sigmoid-shaped behavior curve. Using a linear regression method we found that the dynamic diffusion of the pores obeys a Ginstling-Brownshtein equation which describes a tridimensional diffusion mechanism with spherical symmetry, known as D4 mechanism [27]:

$$[(1 + \alpha)^{1/3} - 1]^2 = k_D t_s \tag{4}$$

where k_D is the equilibrium constant with a value of $k_D = 0.017$, a standard deviation of 0.002 and $r = 0.986$, in the case of the LSBN1 ceramic. The same model applied to the LSBN3 sample gave $k_D = 0.016$, a standard deviation of 0.002 and $r = 0.988$.

In the case of the LSBN5 sample, the maximum values of the measured permittivity vary only slightly with sintering time and remain far below those obtained for the other samples. We must recall that this sample contains additional crystalline phases, which lower the material permittivity according to Wiener's mixture rule [28]. This fact also reaffirms the existence of a solubility limit of the Lanthanum ions in the SBN solid solution, deteriorating the dielectric [13] and pyroelectric [14] properties of the material once this limit is exceeded.

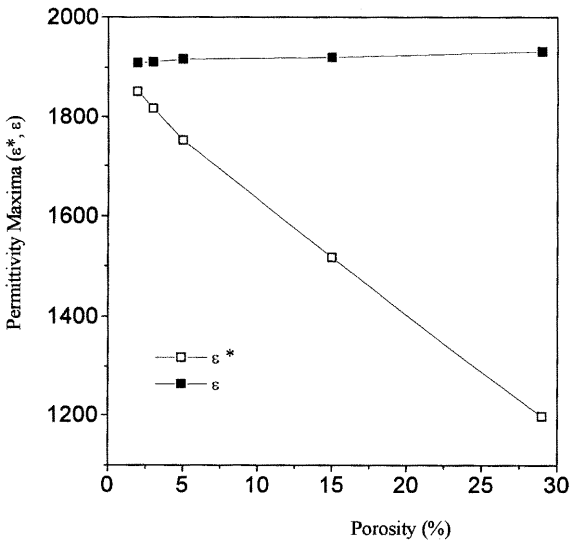

Fig. 7. Porosity dependence of the maximum $\varepsilon(\ p = 0)$ (without pores) and measured ε^* permittivity for the $Sr_{0.285}La_{0.01}$-$Ba_{0.7}Nb_2O_6$ (LSBN1) ceramic. It can be seen that remains approximately constant, suggesting that the increase in ε^* during the material sintering process is due to a decrease in the porosity rather than to a grain size variation.

4. Conclusions

The preparation process and the characterization of a La-doped SBN system was reported in this work. Single phase compounds of LSBN1 and LSBN3 ceramics were obtained. The lattice parameter **a** increases with the La content while **c** remains constant. The grain size remained in the range of 1–2 μm, over all the sintering times applied in this experiment and did not change with the Lanthanum content. The densification rate calculated over different time intervals in the LSBN1 ceramic decreases from 0.66 in the 1–3 h range to 0.15 for 3 to 5 h. For a sintering time of 3 h, a highly dense material with porosity values below 5% was obtained for LSBN1, while LSBN3 required 5 h of sintering time to reach a comparable degree of densification.

The maximum values of the permittivity for LSBN1 and LSBN3 compositions rose monotonically with sintering time due to a decrease in the porosity. The diffusion mechanism of the pores responds to a tridimensional diffusive (D4) process, with $k_D = 0.017$ for LSBN1 and $k_D = 0.016$ for LSBN3 ceramics.

For the LSBN5 sample, $SrNb_2O_6$ and $BaNb_2O_6$ phases coexisted with that of SBN. These additional phases appear to be responsible for the deterioration of the material properties. Accordingly, higher losses and lower densities and permittivities than those of the other studied compositions are obtained. All the above mentioned results point out to the existence of a solubility limit of the Lanthanum ions in the SBN solid solution.

Acknowledgments

This work was partially supported by CoNaCyT Proj. No. 26314E and DGAPA-UNAM Proj. No. IN115098. The authors are grateful to Dr. J. M'Peko for his help in the revision of the manuscript. We thank, I.Gradilla, and E. Aparicio for their technical help. A. Fundora thanks the Foreign Ministry of México for its support.

References

1. M.E. Lines and A.M. Glass, *Principles and Applications of Ferroelectrics and Related Materials* (Claredon Press, Oxford, 1977).
2. A.M. Glass, *J. Appl. Phys.*, **40**, 4699–4713 (1969).
3. Y. Xu, *Ferroelectric Materials and Their Applications* (Elsevier Science Publisher B.V., New York, 1991).
4. A.M. Glass, *Appl. Phys. Let.*, **13**, 147–149 (1968).
5. S.T. Liu and R.B. Maciolek, *J. Electr. Mater.*, **4**, 91–100 (1975).
6. D.J. Mosse, et. al., *Proc. IEEE*, **59**(11), 1628–1629 (1971).
7. K.K. Deb, *Materials for Smart Systems Symposium*, Boston, MA, USA, 127–135 (1994).
8. P. Leiding, M. Villegas, C. Moure, and J.J. Fernández, *Proceedings of the Conference on Electronic Ceramics and Applications*, Electroceramic V, Ed. Department of Ceramic Engineering, University of Aveiro, Portugal, Book-1, 251–254 (1996).
9. M. Ohno and K. Takagi, *Appl. Phys. Let.*, **64**(13), 1620–1622 (1964).
10. D.J. Jendritza, P. Stephan, and H. Janocha, *Proceeding of the Conference on Electronic Ceramics and Applications*, Electroceramic V, Ed. Department of Ceramic Enginnering, University of Aveiro, Portugal, Book-1, 133–136 (1996).
11. X.H. Wan, J.B. Zou, X.Z. Wang, and X.L. Zhang, *Proceeding of the Conference on Electronic Ceramics and Applications*, Electroceramic V, Ed. Department of Ceramic Enginnering, University of Aveiro, Portugal, Book-1, 127–130 (1996).
12. H. Takenchi, S. Jyomura, and C. Nakuya, *Jpn. J. Appl. Phys.*, **24** Supplement 24–2, 36–40 (1985).
13. F. Guerrero, J.J. Portelles, I. González, A. Fundora, H. Amorín, J. Siqueiros, and R. Machorro, *Solid State Communication*, **101**(6), 463–466 (1997).
14. H. Amorín, F. Guerrero, J. Portelles, I. González, A. Fundora, J. Siqueiros, and J. Valenzuela, *Solid State Communication*, in press (1998).

15. R.W. Moulson, *Fundamentals of the Physics Ceramic* (Ed Pergamon Press, New York, 1990).
16. S.H. Nishiwaki, J. Takahashi, and K. Kodeira, *Jpn. J. Appl. Phys*., **33**, 5477–5481 (1994).
17. K. Nagata, Y. Yamamoto, H. Igarashi, and K. Okazaki, *Ferroelectrics*, **38**, 853–856 (1981).
18. T. Tsang, W. Nantiu, and F. Fuhshan, *J. Mater. Sci. Lett*., **13**, 1746-1748 (1994).
19. R.B. Atkin and R.M. Fulrath, *J. Am. Ceram. Soc*., **54**(5), 265–270 (1971).
20. Q.Y. Jiang and L.E. Cross, *J. Mat. Sci*., **28**, 4536–4543 (1993).
21. PC-APD Windows Software for Automated Powder Diffraction, User's Guide, Second Edition, 1994 Copyright© Philips Electronics N.V. 1993.
22. R.B. Maciolek and S.T. Liu, *J. Electr. Mater*., **4**, 517 (1975).
23. R.L. Coble, *J. Appl. Phys*., **32**(5), 787–792 (1961).
24. F. Abad El Salam, A. Tawfik, and A.I. Eatah, *Ferroelectrics*, **65**, 131–141 (1985).
25. Y. Sato, H. Kanai, and Y. Yamashita, *Jpn. J. Appl. Phys*., **33**, 1380–1384 (1994).
26. W. Wersing, K. Lubit, and J. Mohaupt, *Ferroelectrics*, **68**, 77 (1986).
27. F. Amar, J. Bernhoic, B. Sthephan, J. Jellinek, and P.J. Salamon, *J. Appl. Phys*., **65**(8), 3219–3225 (1989).
28. R.C. MacKenzie, *Differential Thermal Analysis* (Academic Press, London, 1972).
29. I.T. Tareev, *Física de los Materiales Dieléctricos* (Ed Mir, Moscú, 1975).